RESEARCH PAPER

Insight into the mechanism of microbially induced carbonate precipitation treatment of bio-improved calcareous sand particles

Bo Zhou[1] · Xing Zhang[1] · Jianfeng Wang[2] · Huabin Wang[1] · Jiawei Shen[1]

Abstract

The use of the calcareous soil as a backfill material in ocean constructions faces pervasive challenges due to the significant rate of particle fracture. To meet the requirements of marine ecological protection, a bio-cementing technique, microbially induced carbonate precipitation (MICP), has emerged as a green method for improving the soil properties of calcareous sands. This paper presents a detailed study on the effect of MICP on the fracture behaviours of calcareous particles and its treating mechanism at microscopic scale level. First, individual calcareous and dolomite particles were treated by MICP for different numbers of rounds. The increase ratio of the particle mass and the filling degree of the intra-particle pores were then measured to evaluate the treatment effect of MICP on individual sand particles. Combining with scanning electron microscopy measurements of the evolution of the particle morphology and internal microstructures of the calcareous particles, the intra-particle pore filling effect as well as the surface coating effect induced by MICP treatment were directly observed. Finally, a series of single-particle crushing tests indicated that the intra-particle pore filling effect of MICP rather than the surface coating effect played the dominant role in improving the fracture pattern and fracture strength of calcareous sand particles.

Keywords Calcareous sand · Intra-particle pore structure · Microbially induced carbonate precipitation · Particle fracture · Treatment effect

1 Introduction

Calcareous sands are primarily composed of calcium carbonate minerals, and they are widely distributed in the warm and shallow seas of the world's tropical and subtropical regions. As calcareous sediments are mainly formed by the weathering of the skeletal remains of marine organisms, such as corals, foraminifera and shells, calcareous sands are characteristic of complex particle morphologies and abundant intra-particle pores. As a result, they usually exhibit distinct mechanical properties from those of ordinary quartz sands. For example, although the complex-shaped particles of calcareous sands form a loose

fabric within the soil structure, the inter-particle locking effect usually results in a high internal friction angle at low stress conditions [3, 5]. More significantly, due to the weak intra-particle pore structure, calcareous sands are highly susceptible to particle fracture and degradation at high stress conditions [6, 23, 43]. Therefore, calcareous sands are regarded as 'special soils' in most engineering applications.

With the development of offshore and oceanic engineering, calcareous sands have become the most commonly used backfilling materials for reclamation work, building foundations, road embankments and airport runways. However, the significant rate of particle fracture when using such sands gives rise to a large number of difficult engineering problems, such as the inadequate bearing capacity of foundations and drilling piles and the overlarge settlement of road embankments and airport runways under cyclic loading [2, 15, 16]. Moreover, the fine contents of calcareous sands, with a loose fabric and a high saturation, are highly vulnerable to soil liquefaction during

✉ Bo Zhou
zhoubohust@hust.edu.cn

1 School of Civil and Hydraulic Engineering, Huazhong University of Science and Technology, Wuhan, China

2 Department of Architecture and Civil Engineering, City University of Hong Kong, Hong Kong, China

earthquakes [33, 45, 46]. To solve these engineering problems, it is necessary to improve the mechanical properties of calcareous sands through reinforcing techniques, such as mechanical compaction [38], chemical grouting [44], cement grouting [34] and geotextile reinforcement [41]. As ocean engineering sites are located far offshore, these conventional terrestrial methods for soil improvement are restricted by the need for mechanical equipment, material transport and suitable construction environments. More importantly, chemical and cement grouting may cause serious oceanic pollution and damage the marine ecological environment. Therefore, an innovative and environmentally friendly soil improvement method for calcareous sands is urgently needed for the development of offshore and ocean engineering.

Recently, a bio-cementing technique, microbially induced carbonate precipitation (MICP), has emerged as a 'green' geotechnical method for the improvement of ground soil. A widely applied MICP process is based on urea hydrolysis by *Sporosarcina pasteurii*, a microbe with strong activity in natural soils, even in acidic and saline environments [1, 4, 9, 17, 20, 27, 45]. These bacteria can hydrolyse urea into carbonate ions with high efficiency, then rapidly produce calcite crystals in a calcium source environment. The MICP process can be expressed by the following equations.

$$CO(NH_2)_2 + 2H_2O \rightarrow 2NH_4^+ + CO_3^{2-} \tag{1}$$

$$Ca^{2+} + CO_3^{2-} \rightarrow CaCO_3(solid) \tag{2}$$
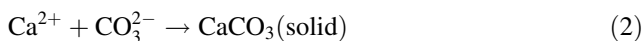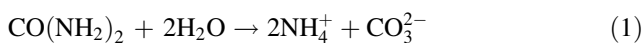
The earlier applications of MICP for soil improvement were mainly applied to the commonly used quartz sands [1, 4, 7, 31, 35]. Recently, MICP treatment has also been applied to the soil improvement in marine calcareous sands [8, 10, 18, 19, 21, 47, 48]. A large number of experimental studies have confirmed that MICP treatment produces calcite cement inside the soil matrix, thereby reducing the permeability and improving the stiffness and strength for both kinds of granular soils. Subsequently, successful applications in field tests have proven that MICP treatment is a promising method to reduce the settlement and enhance the bearing capacity and liquefaction resistance of foundations [12, 26, 30, 42, 45]. Close inspection of the literature reveals that research on MICP has mainly focused on the optimisation of treatment techniques and the evaluation of treatment effects on soil properties. These studies have reported several difficult challenges to the application of MICP, such as the spatial heterogeneity of calcite precipitation inside the treated samples [24, 32, 36] and the brittle failure of the treated samples, which have very low residual strengths under loading [4, 7, 19, 22].

An understanding of the microscopic mechanism of MICP treatment holds the key to meeting these challenges and rationalising the different treatment effects on quartz sands and calcareous sands. For quartz sands, it is generally believed that MICP produces a calcite coating on the particle surface and a calcite filling into inter-particle pores, which result in calcite cementing or bridging between the contacting particles [7, 28, 37]. This greatly enhances the soil stiffness and strength. Due to the critical role of particle fracture in determining the mechanical properties of granular soils, such as compressibility, shear strength and critical state behaviours [6, 23, 43], the effect of MICP on the particle fracture of granular soils is an important scientific issue; however, it has rarely been addressed. Xiao et al. reported that MICP treatment substantially restrained the particle breakage of quartz sands [47]. They attributed the treatment mechanism to the extra energy dissipation induced by the inter-particle calcite debonding, rather than to the enhancement of particle fracture strengths. With regard to calcareous sands, the abundant surface holes and intra-particle pores provide favourable biochemical environments for bacterial adsorption and calcite precipitation, and the mechanism of MICP is more complicated than that for quartz sand. Moreover, the effect of the intra-particle pore filling induced by MICP on the fracture behaviours of calcareous particles themselves, and the underlying mechanism of particle fracture, remain unclear. Therefore, a key scientific question is arisen: How to quantify the intra-particle filling effect by MICP treatment on the mitigation of the particle crushing nature of calcareous sands.

The objective of this study was to investigate the effect of MICP on the fracture behaviours of calcareous sand particles and to deduce its treating mechanism at microscopic scale level. Individual calcareous particles were first treated by MICP for different numbers of rounds. To distinguish between the surface coating effect and intra-particle pore filling effect of MICP, dolomite particles without intra-particle pores were chosen as the control group. The particle mass and the filling degree of intra-particle pores of different types of sand particles were investigated as a function of the number of treatment rounds. Scanning electron microscopy (SEM) measurements of the evolution of the particle morphology and internal microstructures provided further evidence of the treatment mechanisms of MICP. Finally, a series of single-particle crushing tests were conducted to investigate the diverse effects of MICP treatment on the fracture strength and fracture pattern of different types of sand particles.

2 Microbially induced carbonate precipitation

2.1 Tested sand particles

The calcareous sand chosen in this study was sampled from the Spratly islands of the South China Sea [50]. Since the insignificant contribution of shell deposits, a total of 210 particles without shells were randomly selected from the screening packing, with the size ranging from 2.0 to 5.0 mm. To help distinguish the treatment effect and mechanism of MICP specifically for calcareous sand particles, a control group of 210 dolomite particles with the same size range was chosen. As shown by the photographs in Fig. 1, calcareous particles have more irregular and concave shapes than dolomite particles. The SEM images in Fig. 1 further show that calcareous particles have abundant surface concavities and intra-particle pores, which are due to their bio-geological origin from coral reef and reef limestone, whereas dolomite particles are intact without surface concavities and intra-particle pores. In addition, the SEM image of dolomite particles features clear rhombohedral crystals; in contrast, no clear crystals can be identified from the SEM image of calcareous

particles at the current scale level because the mineral of calcareous particles is always microcrystalline or cryptocrystalline due to its biological origin [25]. Therefore, in the following sections, the crystal shape observed in SEM images combined with the mineral phase measured by X-ray diffraction (XRD) results are regarded as two important indicators to distinguish between the original mineral of calcareous particles and the newly produced mineral by MICP.

2.2 MICP treatment procedures

In this study, a commonly used bacterium, *Sporosarcina pasteurii* (ATCC 11,859) was selected for the MICP treatment. The bacterial cells from the frozen stock were first grown in a liquid medium containing 20 g/L yeast extract (NH_4-YE), 10 g/L NH_4Cl, 12 mg/L $MnSO_4 \cdot H_2O$ and 24 mg/L $NiCl_2 \cdot 6H_2O$ at a pH of 8.5 and a temperature of 30 °C. After 24-h culture, the optical OD_{600} value of the obtained bacterial suspension (BS) was measured at a wavelength of 600 nm by an ultraviolet spectrophotometer, reaching an ultimate range of $OD_{600} = 1.2–1.8$. The average urease activity of the bacteria was quantified by the electrical conductivity, which was approximately 3.5–5.3 mM urea hydrolysed/min. Referring to recent
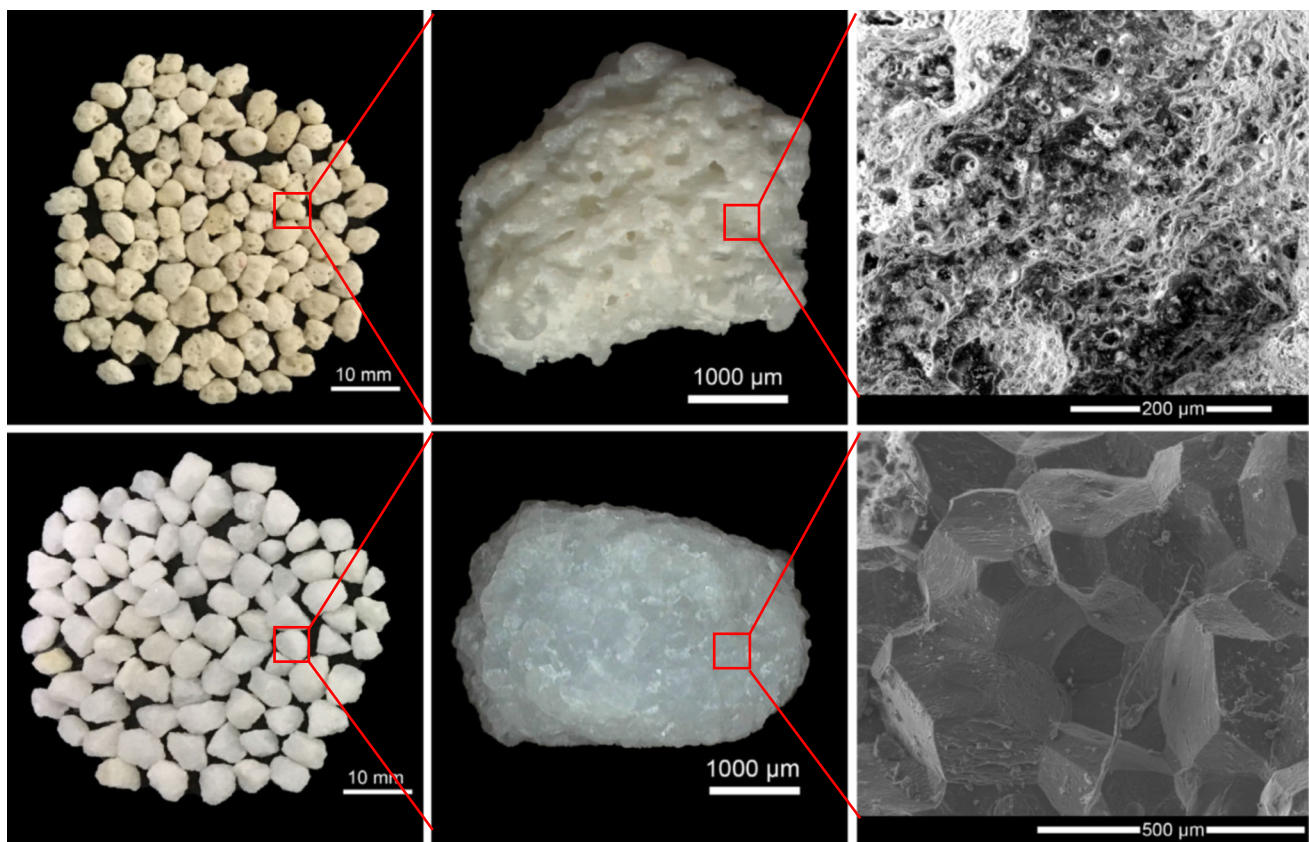

Fig. 1 Photographs and SEM images of the tested calcareous particles (upper row) and dolomite particles (lower row)

studies [1], the cementation solution (CS) for the MICP treatment in this study was a mixture of urea (CON_2H_4) and $CaCl_2$, and the concentration of each is about 0.5 mol/L after mixing.

To directly investigate the mechanism by which MICP treatment affects particle fracture behaviours, the above-described sand particles were separately treated by MICP and then tested by single-particle crushing tests. The 210 particles of each kind were divided into seven groups of 30 particles each. The first group was the control group without MICP treatment. From group two to group seven, the number of rounds of MICP treatment was successively increased by one as the group number increased. Figure 2 illustrates the detailed process of one round of MICP treatment. The main procedures are as follows: (1) placing the tested particles separately into a polystyrene culture plate with 48 holes; (2) adding 0.5 mL BS into each hole to immerse each particle; (3) placing the culture plate in an incubator at a temperature of 30 °C for 24 h; (4) transferring these particles into a new culture plate inside the incubator; and(5) injecting 0.5 ml CS at the first time and then 0.25 mL CS each day for 3 days into each hole to trigger carbonate precipitation within each particle. In total, one round of MICP treatment of a particle included 24 h of immersion in BS and 96 h of exposure to CS. Figure 3 shows the morphologies of a calcareous particle and a
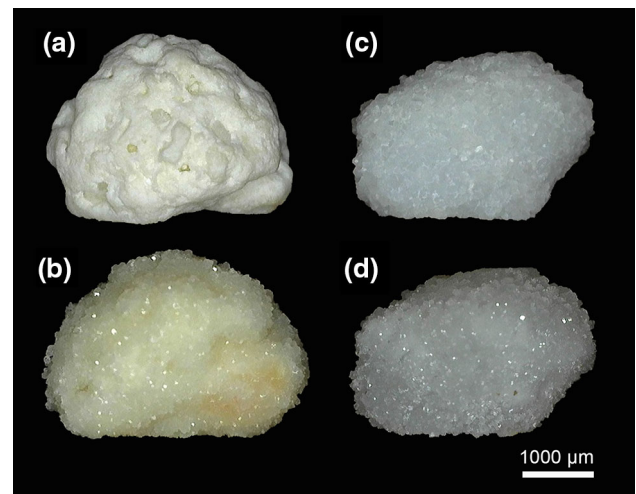

Fig. 3 Morphologies of a calcareous particle ((**a**) and (**b**)) and a dolomite particle ((**c**) and (**d**)) before and after MICP treatment

dolomite particle before and after five rounds of MICP treatment. It can be observed that plentiful calcite crystals were produced around the particle profile, forming a thick calcite coating. This indicated the effectiveness of the proposed MICP technique for treating individual sand particles.
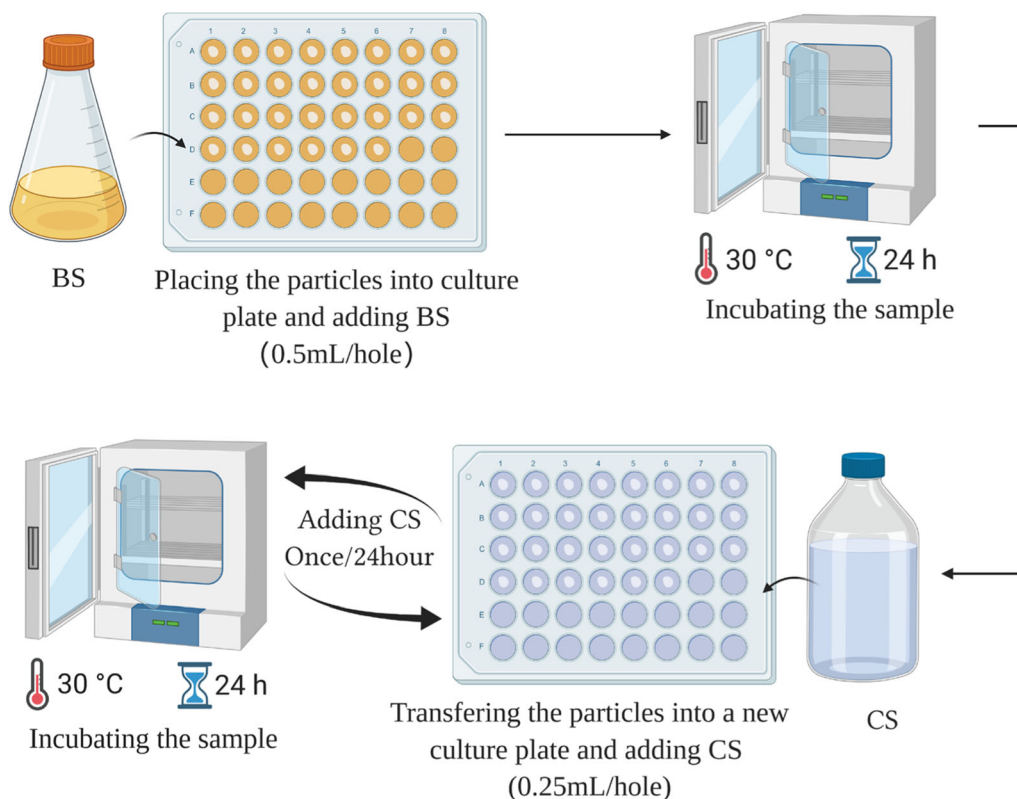

Fig. 2 Schematic diagram of procedures of one round of MICP treatment

3 Treatment effect and mechanism

3.1 Treatment effect

Particle mass growth due to carbonate precipitation is an important indicator of the treatment effect of MICP [4, 13, 39]. To quantify the particle mass growth, the increase ratio (IR) of particle mass was calculated as

$$\mathrm{IR} = \frac{M - M_0}{M_0} \tag{3}$$

where M_0 is the original mass of an untreated particle and M is the mass of the particle after MICP treatment. To measure M, the particle samples were washed by deionized water to remove the by-products after MICP treatment, and then completely dried at the 60 °C condition. As calcareous particles are rich in intra-particle pores, the density variation of the overall particle volume is an essential indicator of the degree to which MICP causes filling of the intra-particle pore structure. Therefore, another index, the filling degree (FD) of intra-particle pores, was calculated as

$$\mathrm{FD} = \frac{V_0(M - M_0)}{M_0(V - V_0)} \tag{4}$$

where V_0 and V are the convex hull's volume of the tested particle before and after MICP treatment, respectively. As illustrated by Fig. 4, the convex hull's volume was calculated as $0.3abc$, where a, b and c are the long, middle and short axes, respectively, of the particle measured by a vernier caliper. The empirical equation measuring the convex hull's volume was obtained based on the image

analysis of the X-ray micro–computed tomography (μCT) images of 30 calcareous sand particles from the authors' previous study [50]. The measurement of the convex hull's volume was briefly introduced in the Appendix. The reason for choosing the convex hull's volume to calculate FD is that the surface coating comparing with the filling of intra-particle voids has a significant impact on the change of the convex hull. Imaging that the pure filling of intra-particle voids can increase M but not increase V in Eq. 4, thereby obtaining a high value of FD. Therefore, we believe FD can depict the filling degree of intra-particle voids by MICP.

Figure 5 shows the increase ratio of particle mass and the filling degree of intra-particle pores as a function of the number of rounds of MICP treatment. For both calcareous and dolomite particles, the increase ratio of particle mass sharply increased with the number of rounds of MICP treatment, as demonstrated in Fig. 5a. However, the particle mass of the calcareous particles increased much faster than that of the dolomite particles, and the increase ratio of the calcareous particle mass therefore covers a much greater range than that of the dolomite particles. These results can be attributed to the larger specific surface area of calcareous particles with rich surface features, which is beneficial for bacterial enrichment and carbonate precipitation.

As shown in Fig. 5b, the filling degree of the intra-particle pores of the calcareous particles was much higher than that of the dolomite particles, indicating that the intra-particle pore structure-filling effect of MICP was pronounced only for the former. Notably, for the calcareous
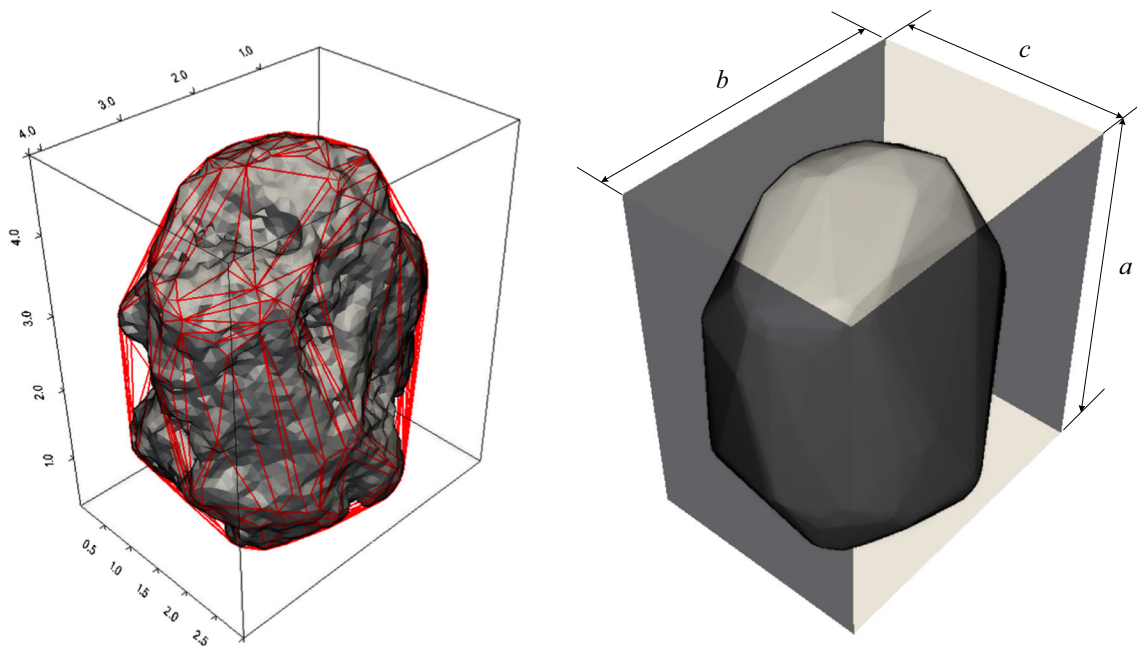

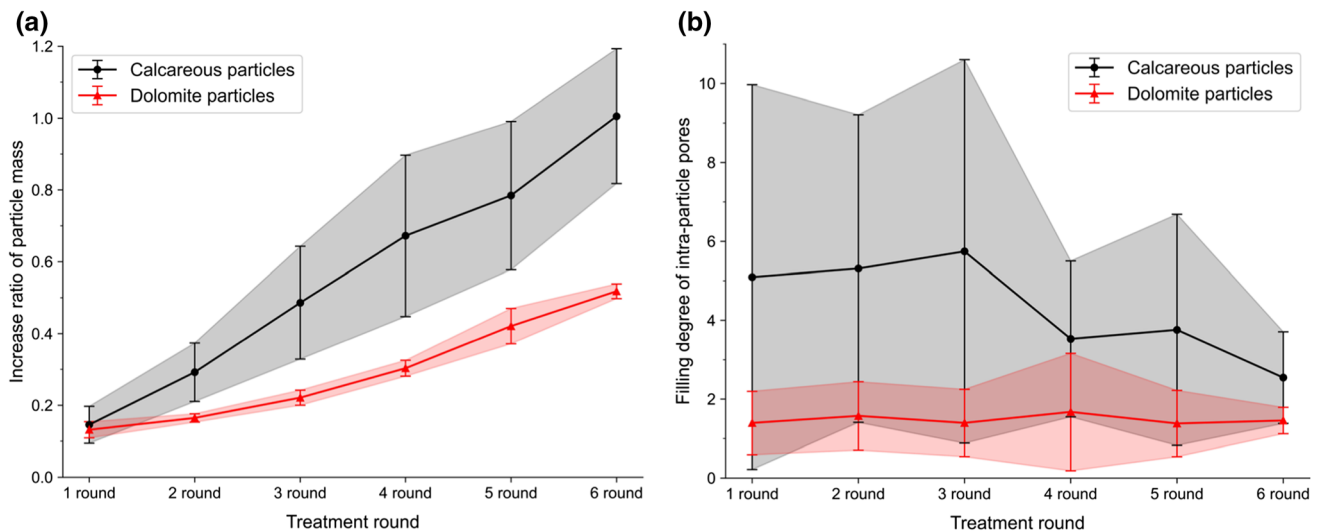**Fig. 4** A calcareous particle and its convex hull (unit: mm)

Fig. 5 Development of the increase ratio of particle mass and filling degree of intra-particle pores of with the increased number of rounds of MICP treatment

particles, the filling degree was high for the first three rounds of MICP treatment and relatively low afterward. In contrast, that of the dolomite particles remained low throughout the process of MICP treatment. This indicated that for calcareous particles, the filling of intra-particle pores was efficient at the earlier stage of MICP treatment, but the efficiency significantly decreased after four rounds of treatment. This might be attributable to the closure of surface concavities and intra-particle pores as a result of filling with calcite. In addition, due to the abundant intra-particle pores and surface concaves, the variable specific surface area of calcareous particles resulted in a high variation of MICP products compared with dolomite particles. In consequence, the calcareous particles have larger error bars than the dolomite particles. The microscopic mechanism of the intra-particle pore filling effect of MICP is discussed in detail in the following section. These results also implied that the coating of particle surfaces gradually replaced the intra-particle pore filling effect as the number of rounds of MICP treatment increased.

3.2 Treatment mechanism

To illustrate the mechanism of intra-particle pore filling by MICP, Fig. 6 shows the X-ray µCT images of a typical calcareous particle, the identified intra-particle pore–throat structure by image analysis and simulated streamlines of fluid flowing across the particle. Detailed information on the µCT scanning, identification of the intra-particle pore–throat structure of calcareous particles and the modelling of the fluid flowing across a calcareous particle can be found in the authors' previous study [50]. It can be seen that the calcareous particle is rich in both surface concavities and

internal pores. By the image analysis of µCT images from the authors' previous study [50], the particle has a measured intra-particle pore porosity of approximately 0.12. In this previous study, calcareous particles with much higher intra-particle pore porosity were identified. The pore–throat network (Fig. 6(b)) reveals the topological connectivity of the intra-particle pore structure, which is a major determinant of the hydraulic conductivity of porous geomaterials. In such a network, fluid streamlines can flow into the deep surface holes and interconnected intra-particle pores, thereby permeating the entire calcareous particle even under a very low seepage pressure (Fig. 6c). These observations therefore indicate that the BS and CS used for MICP treatment can fill the easily accessible interior of the calcareous particle, thereby guaranteeing the condition of MICP process inside its surface concaves and intra-particle pores.

To directly observe the mechanism of intra-particle pore filling by MICP, a calcareous particle sample was crushed after five rounds of MICP treatment and its major fragment was selected for SEM scanning. Figure 7 shows the SEM images of the fracture surface and partial enlarged details of the calcareous particle. Large internal pores can be observed on the fracture surface (Fig. 7a). From the enlarged detail of a particle corner (marked as **A**), two crystal forms can be identified, namely phanerocrystalline and cryptocrystalline. A distinct boundary between these two crystal forms is clearly observed, as marked by the red curve. This represents the boundary between the original particle profile and the newly produced calcite coating formed by MICP treatment. From the enlarged detail of the central area of the fracture surface (marked as **B**), numerous phanerocrystalline crystals can be also seen to densely
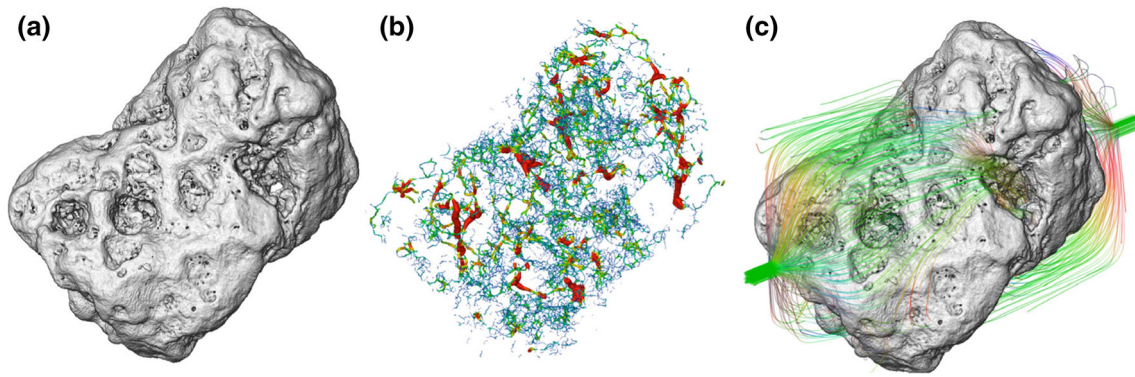
Fig. 6 **a** µCT images of a typical calcareous particle, **b** Pore–throat structure of intra-particle pores, **c** Simulated streamlines of fluid flowing across the particle
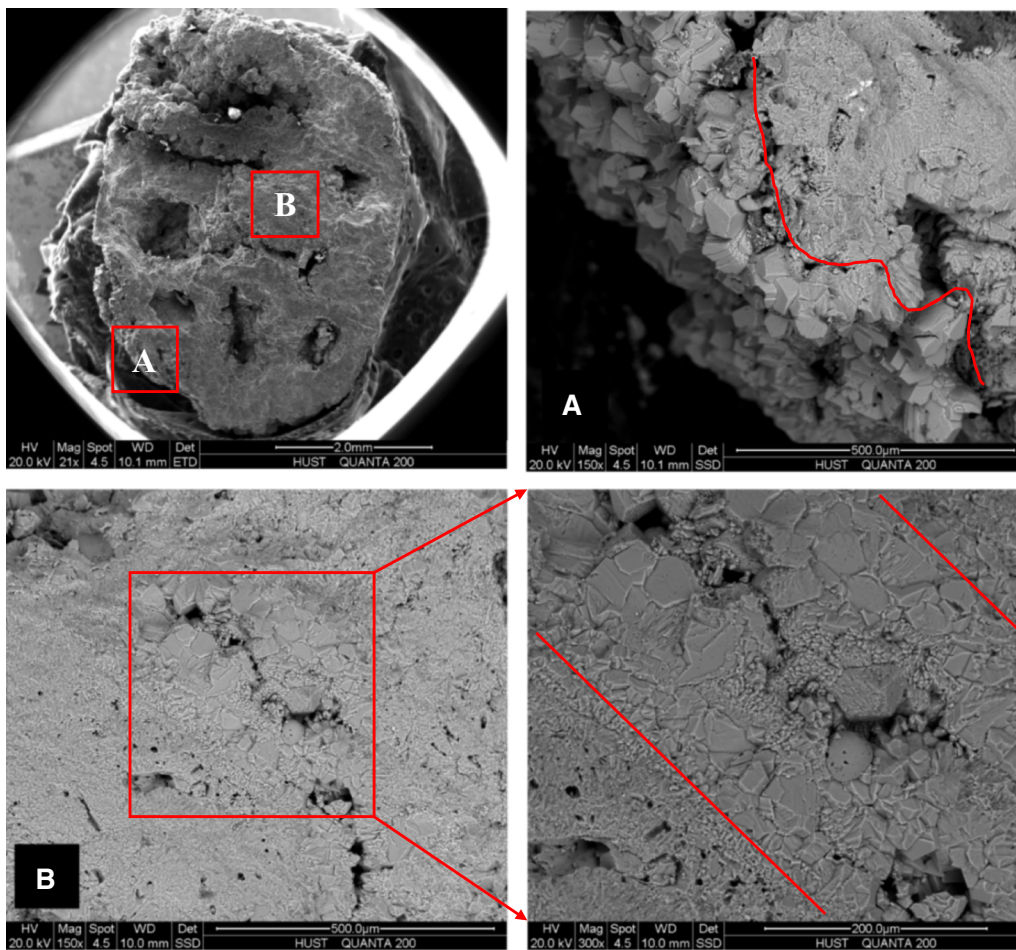

Fig. 7 SEM images of a fracture surface and partial enlarged details of a calcareous particle fragment

accumulate within a narrow band (marked by two red parallel lines in the last subplot), which is probably an original (i.e., pre-treatment) intra-particle pore of the calcareous particle.

To directly prove the intra-particle pore filling was the calcite crystals produced by MICP, XRD phase identification was carried out on the materials located at different areas of the MICP-treated particle. A calcareous particle, a dolomite particle, and the coating and filling materials (from areas A and B in Fig. 7) were separately grinded into powder to prepare three samples for the XRD phase identification. Figure 8 demonstrates the identified mineral phases of these three test materials. The XRD analytical result demonstrated that the main constituent minerals of
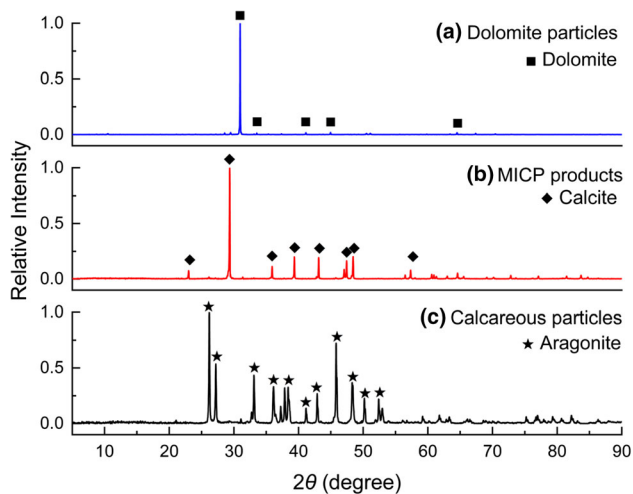
Fig. 8 XRD phase identification of the test materials

the calcareous particle, dolomite particle and MICP product are aragonite, dolomite and calcite, respectively. Combining with the SEM result, this finding directly indicates that MICP induced the intra-particle pore filling of calcareous sands.

4 Particle fracture behaviours

4.1 Particle fracture pattern

The single-particle crushing test is a widely accepted method for investigating the fracture behaviours of granular soil particles [11, 14, 29, 40, 49]. To evaluate the effect of MICP treatment, a series of single-particle crushing tests was conducted to investigate the fracture strength and fracture pattern of the tested particles. Figure 9 shows the loading apparatus used and the loading process of a tested calcareous particle. The apparatus mainly includes a loading frame, a loading system, a load cell, a displacement sensor and a data collection and control system. To conduct a single-particle crushing test, the upper loading platen was actuated by the loading system at a downward speed of 0.1 mm/min to uniaxially compress the particle until major failure. The load cell and the displacement sensor continuously recorded the force and displacement of the upper loading platen. Meanwhile, a high-speed microscope camera was used to capture the fracture process of the particle under loading.

As the MICP treatment produced both a surface coating effect and an intra-particle pore filling effect, the changes in microstructure in terms of particle morphology and intra-particle pore structure had a significant influence on the fracture strength and fracture pattern of the particles subjected to uniaxial compression. Therefore, it is

important to distinguish the roles of these two treatment effects in the change in particle fracture behaviours, and the underlying mechanism of fracture. Figure 10 shows the observed fracture patterns of all the tested particles, and Fig. 11 shows the force–displacement curves of the chosen calcareous and dolomite particles displayed in Fig. 10. Based on the shape of the force–displacement curves, the intensity of the particle fracture and the number of generated fragments, the particle fracture events can be classified into two types, namely major splitting and global comminution.

The particles with the major splitting pattern were characterised by a clear major peak in the force–displacement curve (Fig. 11a), with only two or three large fragments generated after loading (Fig. 10a). The force–displacement curve presented a nonlinear Hertzian-type contact response before the peak and subsequently a brittle failure of the particle after the peak. This fracture pattern mainly occurred for the particles with a regular shape and an intact internal structure. In contrast, for the particles with the global comminution pattern, many minor peaks appeared before the major peak in the force–displacement curve (Fig. 11b), and numerous small fragments were produced during the progressive failure process (Fig. 10b). This fracture pattern is probably attributable to the irregular particle shape and intra-particle pore structure. To evaluate the particle fracture strength, the maximum tensile stress within the particle volume during the loading process was calculated by the following equation [11, 14, 40].

$$\sigma = 0.9 \frac{F_{\max}}{d^2} \tag{5}$$

where $F_{\max}$ is the loading force at the major peak of the force–displacement curve and $d = \sqrt{bc}$ is the equivalent diameter of the tested particle.

Figure 12 shows the proportion of tested particles with different fracture patterns, and boxplots of the fracture strengths of particles with different fracture patterns, as a function of the number of rounds of MICP treatment. For both kinds of tested particles without MICP treatment, the proportion of particles with the global comminution pattern was much larger than that with the major splitting pattern. For calcareous particles, the dominance of the global comminution pattern is mainly attributable to their intra-particle pore structures, whereas for the dolomite particles it can probably be explained by their rough surface textures and weak inter-crystal faces. With successive rounds of MICP treatment, the proportion of the major splitting pattern for both kinds of tested particles gradually increased, whereas that of the global comminution pattern gradually decreased. However, this trend was more pronounced for the calcareous particles. It can be inferred that the intra-particle pore filling effect rather than the surface
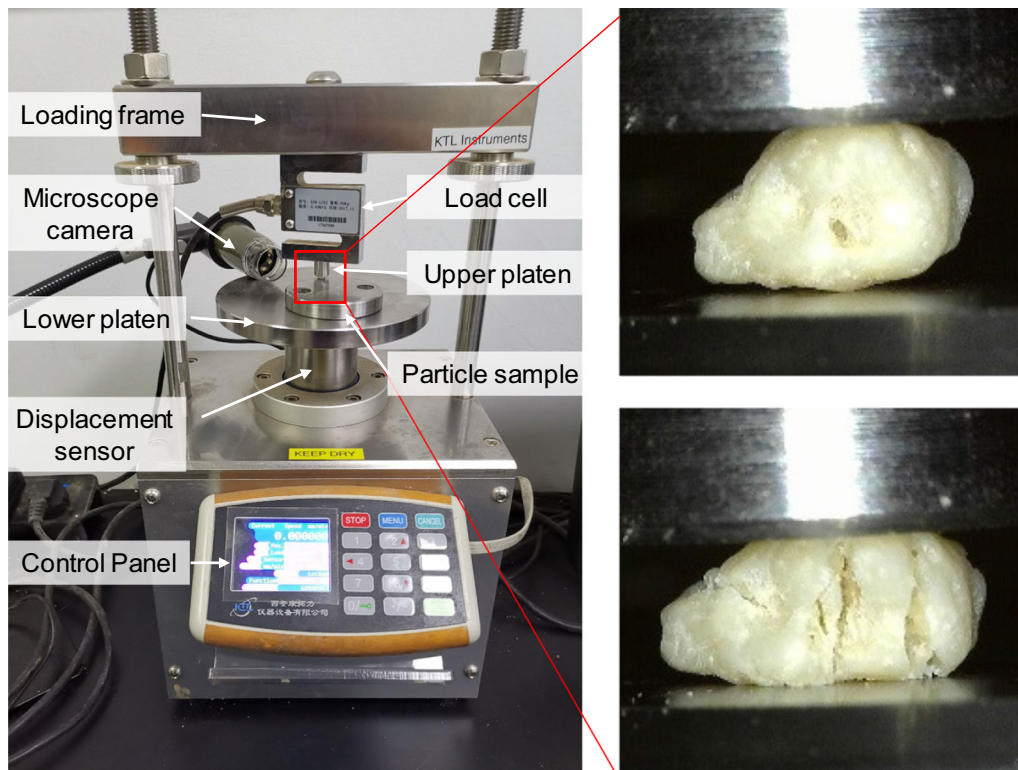
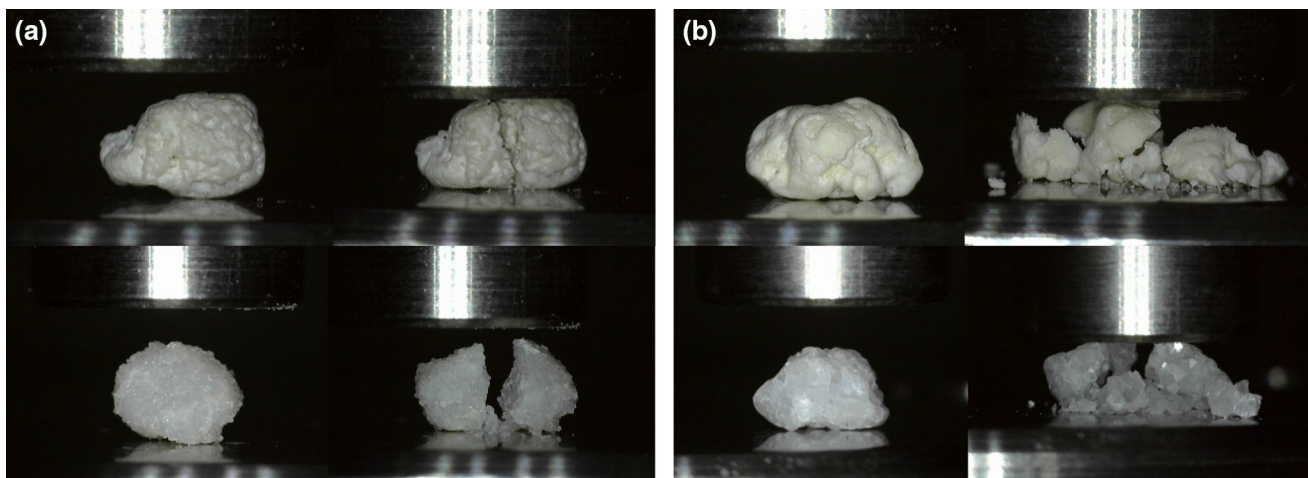**Fig. 9** Loading apparatus used and loading process of a tested calcareous particle

Fig. 10 Fracture patterns of the tested particles: **a** Major splitting and **b** Global comminution

coating effect of MICP makes the greater contribution to strengthening the weak microstructures of sand particles. In addition, it was noticed that the particles with the major splitting pattern had higher average fracture strengths than those with the global comminution pattern. This result also indicated that the transition of the fracture pattern from global comminution to major splitting directly contributed to the reinforcement of the particle fracture strength.

4.2 Particle fracture strength

To investigate the effect of MICP treatment on the particle fracture strength, the distributions of particle survival probability were plotted together with the corresponding Weibull fitting curves of the tested particles with different numbers of rounds of MICP treatment (Fig. 13). The Weibull distribution of particle survival probability for a group of tested particles was fitted by the following equation [11, 14, 40].
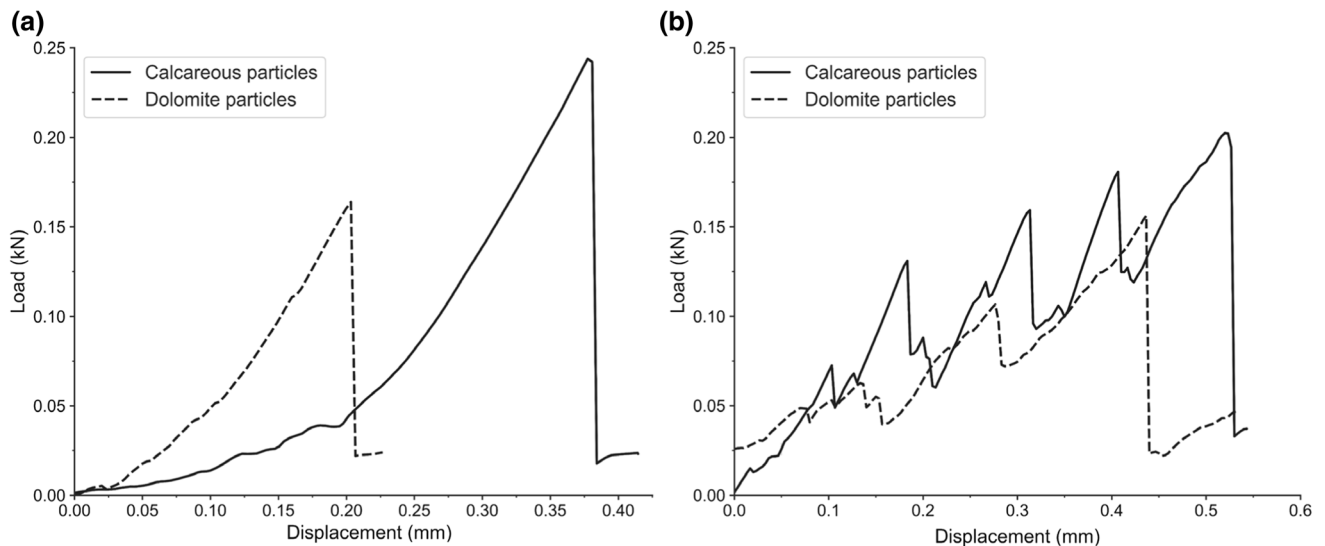
(a)

(b)

Fig. 11 Force–displacement curves of a typical calcareous particle and a typical dolomite particle with different fracture patterns: **a** Major splitting and **b** Global comminution

$$P_s = \exp\left(-\left(\frac{\sigma}{\sigma_0}\right)^m\right) \qquad (6)$$

where P_s is the survival probability of a tested particle with the stress of σ, σ_0 is the obtained characteristic fracture strength of this particle group and m is the obtained Weibull modulus, indicating the variability of the fracture strength of this particle group. σ_0 and m were measured by using a least-squares method on the data points in Fig. 13.

As shown in Fig. 13, the curve of particle survival probability continuously shifts to the right with the increasing number of rounds of MICP treatment, especially for the calcareous particles. This indicates that a particle treated more times had a higher survival probability than a particle treated fewer times when it is subjected to loading, which is evidence for the significant reinforcing effect of MICP on the fracture strength for both kinds of sand particles. However, the rightward shifting of the curves with progressive rounds of MICP treatment differs notably between the two kinds of particles, as described in the next paragraph. This is consistent with the obtained σ_0 and m values of the tested particles as a function of the number of rounds of MICP treatment, as plotted in Fig. 14.

For both kinds of tested particles, σ_0 first increased and then decreased with the increasing number of treatment rounds (see Fig. 14a). Taking calcareous particles for example, σ_0 rapidly increased until the fifth round of MICP treatment but slightly decreased after the sixth round of

MICP treatment. This indicates that the effect of MICP on the particle fracture strength depends on the number of rounds of treatment. This result is consistent with the development of the intra-particle pore filling degree of calcareous particles plotted in Fig. 5b, and it reveals that the limited filling degree of intra-particle pores at the late stage of MICP treatment led to the limited effect of treatment on the particle fracture strength. More importantly, the rate of increase of σ_0 for the calcareous particles was much higher than that for the dolomite particles. This indicates that the intra-particle pore filling effect rather than the surface coating effect of MICP played the dominant role in reinforcing the fracture strength of calcareous sand particles. As demonstrated in Fig. 14b, the m value mostly increased with the increasing number of MICP treatment rounds, especially for the calcareous particles, which indicates that the intra-particle pore filling effect by MICP treatment is beneficial for reducing the variability of particle fracture strengths. However, for dolomite particles, a sharp decrease of m value from four to five treatment rounds was observed, which phenomenon might be resulted from the unstable microstructure of the surface coating calcite produced by MICP treatment. This result is also consistent with the increased proportion of particles exhibiting the major splitting pattern following MICP treatment (see Fig. 12). In conclusion, the intra-particle pore filling effect of MICP can be identified as the
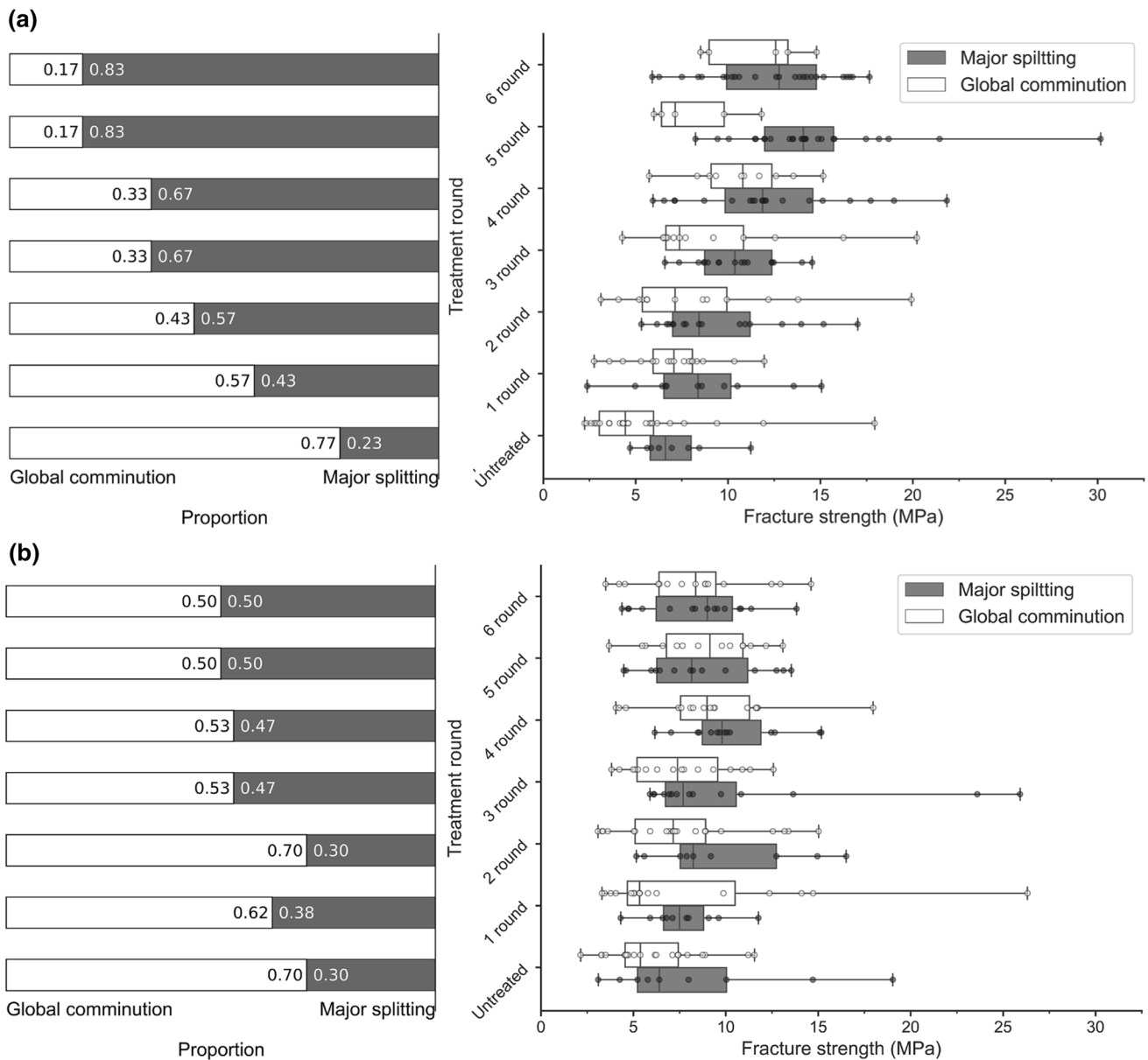
Fig. 12 Proportion of tested particles with different fracture patterns, and boxplots of the fracture strengths of particles with different fracture patterns, with increasing number of rounds of MICP treatment: **a** For calcareous particles and **b** For dolomite particles

fundamental mechanism by which this treatment improves the particle fracture behaviours of calcareous sand particles.

5 Conclusions

Particle fracture plays an important role in determining the macroscopic mechanical properties of calcareous sands. This study investigated the effect of MICP on the fracture behaviours of calcareous particles at particle scale level, which provides a deep insight into understanding the mechanical behaviours and treating effect of MICP-improved calcareous sands. Seven groups of calcareous particles and seven control groups of dolomite particles were treated with different numbers of rounds of MICP. The corresponding effects and mechanisms for the two kinds of sand particles were first discussed based on the development of particle mass and intra-particle pore filling degree as a function of the number of treatment rounds, and by the
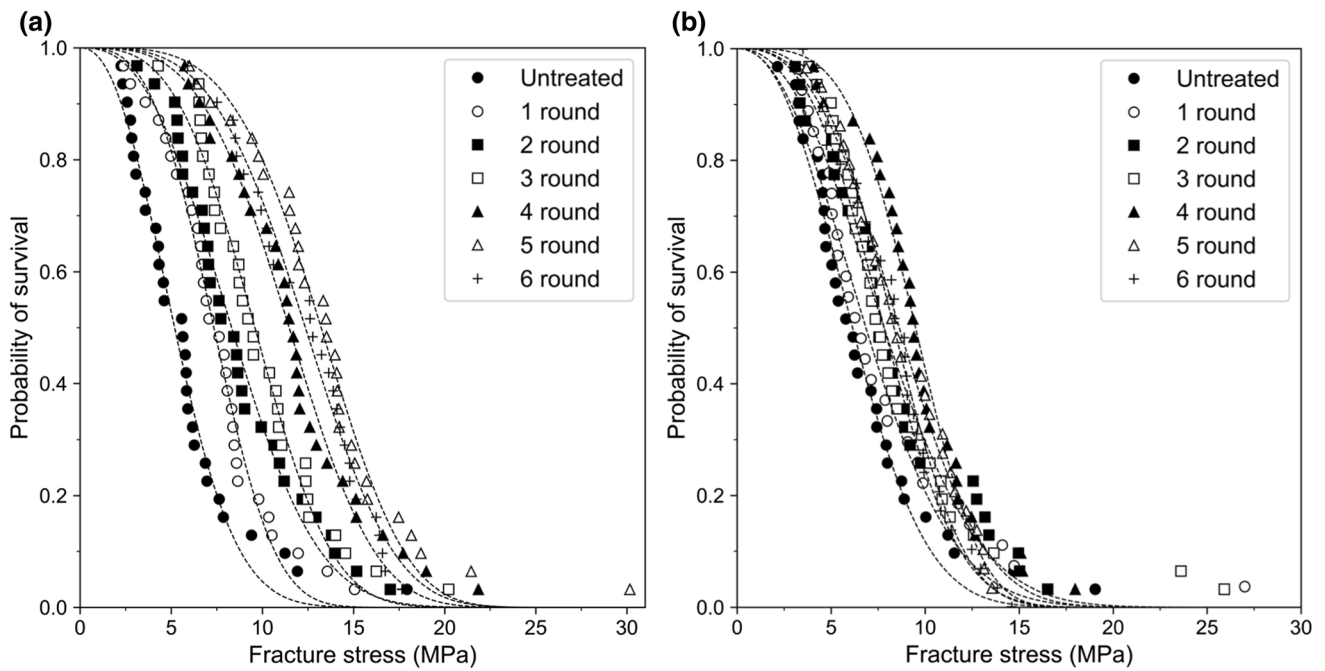
Fig. 13 Distributions of the particle survival probability and the corresponding Weibull fitting curves of the tested particles with different numbers of MICP treatment rounds, **a** For calcareous particles and **b** For dolomite particles
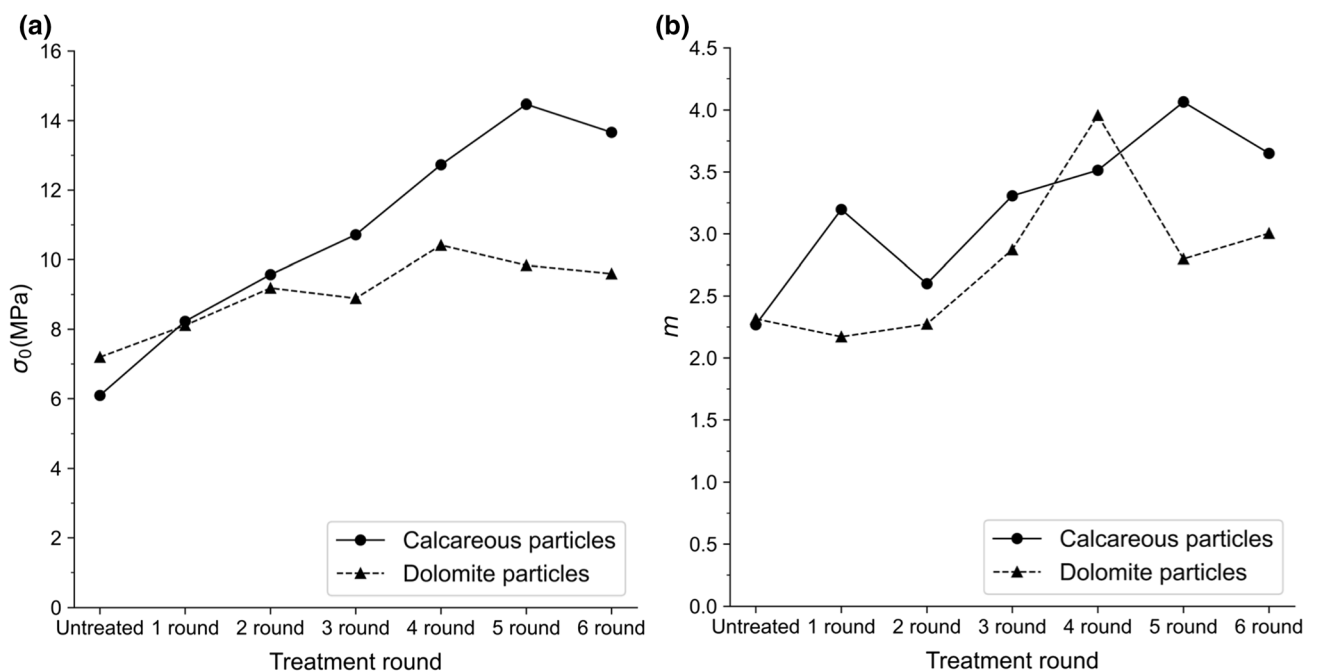

Fig. 14 a Characteristic fracture strength and **b** Weibull modulus of the tested particles as a function of the number of MICP treatment rounds

analysis of SEM images. The effect of MICP treatment on the fracture behaviours of the tested particles was carefully investigated based on a series of single-particle crushing tests. Three major conclusions are summarised below:

(1)   During MICP treatment, plentiful calcite crystals precipitated around the particle profiles, forming a

thick calcite coating. MICP is therefore a powerful and efficient technique for treating individual sand particles.

(2)   The increase ratio of particle mass sharply increased with the number of rounds of MICP treatment for both the calcareous and dolomite particles, indicating

a significant effect of MICP treatment on both kinds of sand particles. For a given number of treatment rounds, the intra-particle pore filling degree of the calcareous particles was much higher than that of the dolomite particles, indicating that pore filling by MICP treatment was more efficient for the former sand type. Moreover, the analysis of SEM images directly demonstrated that MICP induced the filling of the intra-particle pores of calcareous particles.

(3) With increasing numbers of rounds of MICP treatment, the dominant fracture pattern of both tested particle types gradually transitioned from global comminution to major splitting, and the characteristic fracture strength significantly increased as well. However, the increase in the characteristic fracture strength was much faster for the MICP-treated calcareous particles than for the MICP-treated dolomite particles. The enhancement of the fracture strength of calcareous particles by MICP only continued up to a limited number of treatment rounds. Together, the findings revealed that the intra-particle pore filling effect rather than the surface coating effect of MICP played the dominant role in improving the fracture pattern and fracture strength of the calcareous sand particles.

Appendix: Calculation of convex hull's volume

A convex hull is defined as the minimal region containing all line segments consisting of any two points inside. An intrinsic function in Python3.8 was used to generate the convex hull, and calculate its volume V_{con} of a given particle, as illustrated in Fig. 4. An oriented bounding box (OBB) was obtained based on a principal component analysis (PCA) of all the voxels belonging to the particle volume. The dimensions of the particle a, b and c are the length, width and height of OBB. Figure 15 demonstrates the original morphology and convex hull of 30 calcareous particles. Figure 16 shows the correlation between the convex hull's volume (V_{con}) and the bound box's volume (V_{box}) for all the particles. A well linear relationship with a slope of 0.3 was identified between these two parameters. In practical experiments, a vernier caliper was used to measure the dimensions a, b and c of the tested particle,
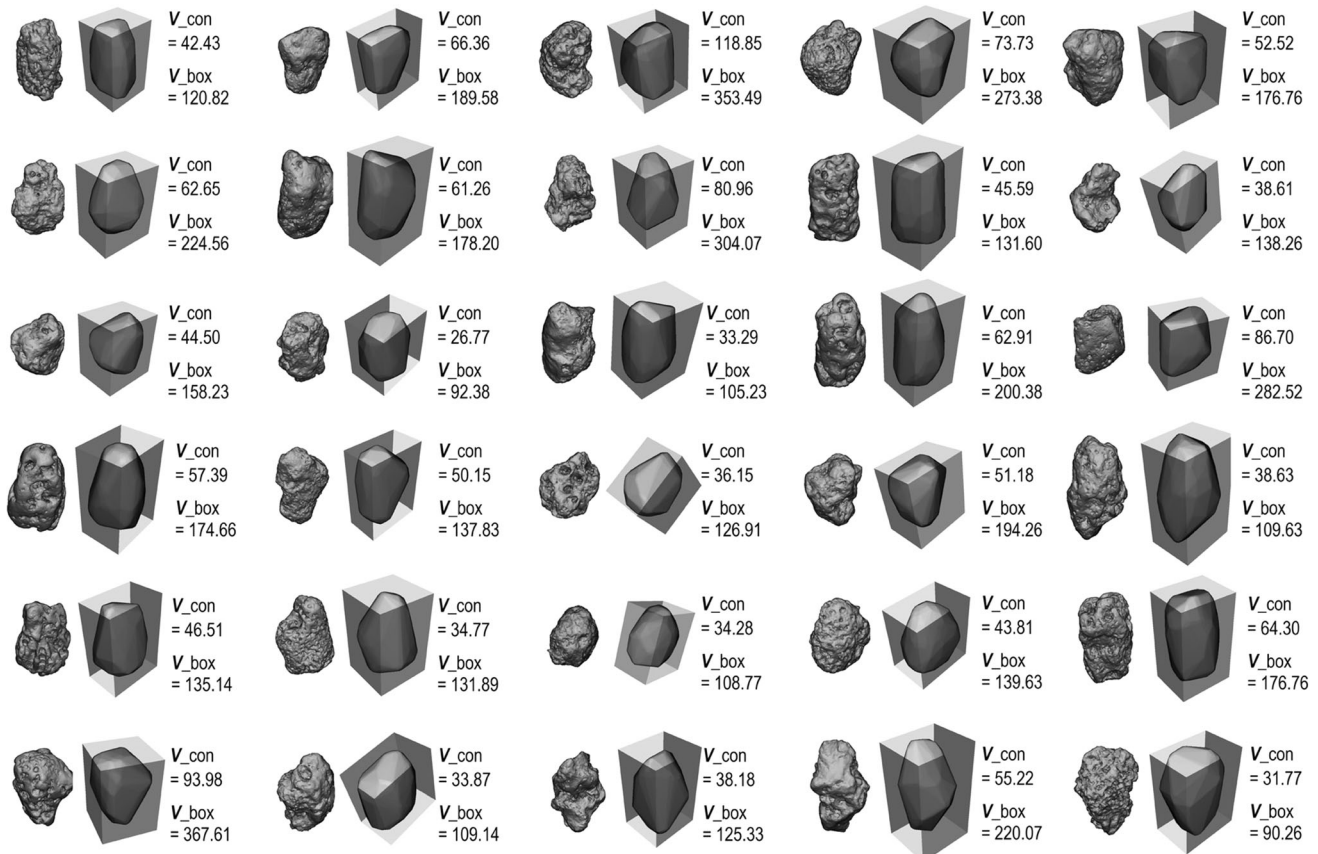

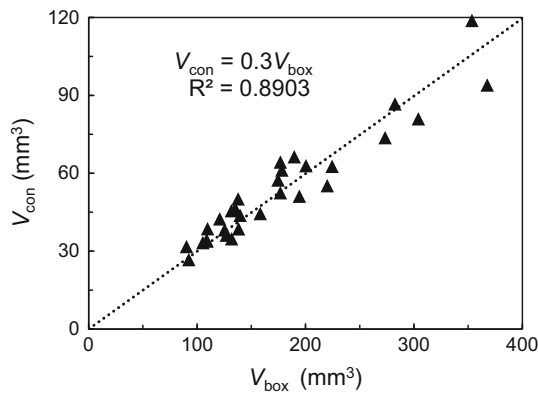**Fig. 15** Morphology and convex hull of 30 calcareous particles

Fig. 16 Relationship between V_{con} and V_{box}

and a uniform empirical equation $V_{con} = 0.3abc$ was adopted to approximately calculate its convex hull's volume.

References

1. Al QA, Soga K (2013) Effect of chemical treatment used in MICP on engineering properties of cemented soils. Géotechnique 63:331–339
2. API (American Petroleum Institute) (2000). Recommended practice for planning, designing, and constructing fixed offshore platforms-working stress design. API Publishing Services, Washington, D.C.
3. Brandes H (2011) Simple shear behaviour of calcareous and quartz sands. Geotech Geolog Eng 29:113–126
4. Cheng L, Shahin MA, Cord-Ruwisch R (2014) Bio-cementation of sandy soil using microbially induced carbonate precipitation for marine environments. Géotechnique 64:1010–1013
5. Coop MR (1990) The mechanics of uncemented carbonate sands. Géotechnique 40:607–626
6. Coop MR, Sorensen KK, Bodas Freitas T, Georgoutsos G (2004) Particle breakage during shearing of a carbonate sand. Géotechnique 54:157–163
7. Cui MJ, Zheng JJ, Zhang RJ, Lai HJ, Zhang J (2017) Influence of cementation level on the strength behaviour of bio-cemented sand. Acta Geotech 12:971–986
8. Cui MJ, Zheng JJ, Chu J, Wu CC, Lai HJ (2021) Bio-mediated calcium carbonate precipitation and its effect on the shear behaviour of calcareous sand. Acta Geotech 16:1377–1389
9. DeJong JT, Soga K, Kavazanjian E et al (2013) Biogeochemical processes and geotechnical applications: progress, opportunities and challenges. Géotechnique 63:287–301
10. Dyer M, Viganotti M (2016) Oligotrophic and eutrophic MICP treatment for silica and carbonate sands. Bioinspir Biomin Nan 6:168–183
11. Fu R, Hu X, Zhou B (2017) Discrete element modeling of crushable sands considering realistic particle shape effect. Comput Geotech 91:179–191
12. Han Z, Cheng X, Ma Q (2016) An experimental study on dynamic response for MICP strengthening liquefiable sands. Earthq Eng Eng Vib 15:673–679
13. He J, Chu J, Gao Y et al (2019) Research advances and challenges in biogeotechnologies. Geotech Res 6:144–155
14. Hu G, Zhou B, Fu R, Guo Y, Han C, Lv K (2021) Discrete element modeling of the compression molding of polymer–crystal composite particles. Powder Technol 390:112–125
15. Jardine R, Chow F, Overy R, Standing J (2005) ICP design methods for driven piles in sands and clays. Thomas Telford
16. Klotz E, Coop M (2001) An investigation of the effect of soil state on the capacity of driven piles in sands. Géotechnique 51:733–751
17. Lai Y, Yu J, Liu S, Liu J, Wang R, Dong B (2021) Experimental study to improve the mechanical properties of iron tailings sand by using MICP at low pH. Constr Build Mater 273:21729
18. Liu L, Liu H, Xiao Y, Chu J, Xiao P, Wang Y (2018) Biocementation of calcareous sand using soluble calcium derived from calcareous sand. Bull Eng Geol Environ 77:1781–1791
19. Liu L, Liu H, Stuedlein AW, Evans TM, Xiao Y (2019) Strength, stiffness, and microstructure characteristics of biocemented calcareous sand. Can Geotech J 56:1502–1513
20. Liu B, Zhu C, Tang CS, Xie YH, Yin LY, Cheng Q, Shi B (2020) Bio-remediation of desiccation cracking in clayey soils through microbially induced calcite precipitation (MICP). Eng Geol 264:105389
21. Liu KW, Jiang NJ, Qin JD, Wang YJ, Tang CS, Han XL (2021) An experimental study of mitigating coastal sand dune erosion by microbial-and enzymatic-induced carbonate precipitation. Acta Geotech 16:467–480
22. Lv C, Zhu C, Tang CS, Cheng Q, Yin LY, Shi B (2021) Effect of fiber reinforcement on the mechanical behavior of bio-cemented sand. Geosynth Int 28:195–205
23. Miao G, Airey D (2013) Breakage and ultimate states for a carbonate sand. Géotechnique 63:1221–1229
24. Minto JM, Lunn RJ, El Mountassir G (2019) Development of a reactive transport model for field-scale simulation of microbially induced carbonate precipitation. Water Resour Res 55:7229–7245
25. Montaggioni LF, Braithwaite CJR (2009) Chapter Eight Reef Diagenesis. Dev Mar Geol 5:323–372
26. Montoya BM, DeJong JT, Boulanger RW (2013) Dynamic response of liquefiable sand improved by microbial induced calcite precipitation. Géotechnique 63:302–312
27. Montoya BM, DeJong JT (2015) Stress-strain behavior of sands cemented by microbially induced calcite precipitation. J Geotech Geoenviron Eng 141:04015019
28. Mujah D, Shahin MA, Cheng L (2017) State-of-the-art review of biocementation by microbially induced calcite precipitation (MICP) for soil stabilization. Geomicrobiol J 34:524–537
29. Nakata AFL, Hyde M, Hyodo H, Murata (1999) A probabilistic approach to sand particle crushing in the triaxial test. Géotechnique 49:567–583
30. Nassar MK, Gurung D, Bastani M et al (2018) Large-scale experiments in microbially induced calcite precipitation (MICP): Reactive transport model development and prediction. Water Resour Res 54:480–500
31. van Paassen LA, Ghose R, van der Linden TJ, van der Star WR, van Loosdrecht MC (2010) Quantifying biomediated ground improvement by ureolysis: large-scale biogrout experiment. J Geotech Geoenviron Eng 136:1721–1728
32. Rong H, Qian CX, Li L (2012) Study on microstructure and properties of sandstone cemented by microbe cement. Constr Build Mater 36:687–694
33. Shahnazari H, Jafarian Y, Tutunchian MA, Rezvani R (2016) Probabilistic assessment of liquefaction occurrence in calcareous

fill materials of Kawaihae Harbor. Hawaii Int J Geomech 16:05016001

34. Shen J, Dongsheng XU, Liu Z, Wei H (2020) Effect of particle characteristics stress on the mechanical properties of cement mortar with coral sand. Constr Build Mater 260:

35. Terzis D, Bernier-Latmani R, Laloui L (2016) Fabric characteristics and mechanical response of bio-improved sand to various treatment conditions. Geotech Lett 6:50–57

36. Terzis D, Laloui L (2018) 3-D micro-architecture and mechanical response of soil cemented via microbial-induced calcite precipitation. Sci Rep 8:1–11

37. Terzis D, Laloui L (2019) A decade of progress and turning points in the understanding of bio-improved soils: A review. J Geotech Geoenviron Eng 19:100116

38. Wang XZ, Jiao YY, Wang R, Hu MJ, Meng QS, Tan FY (2011) Engineering characteristics of the calcareous sand in Nansha Islands, South China Sea. Eng Geol 120:40–47

39. Wang Y, Soga K, DeJong JT, Kabla AJ (2021) Effects of bacterial density on growth rate and characteristics of microbial-induced CaCO3 precipitates: Particle-scale experimental study. J Geotech Geoenviron Eng 147:04021036

40. Wang W, Coop MR (2016) An investigation of breakage behaviour of single sand particles using a high-speed microscope camera. Géotechnique 66:984–998

41. Wei H, Zhao T, Meng Q, Wang X, He J (2018) Experimental evaluation of the shear behavior of fiber-reinforced calcareous sands. Int J Geomech 18:04018175

42. Van Wijngaarden WK, Vermolen FJ, Van Meurs GAM, Vuik C (2011) Modelling biogrout: a new ground improvement method based on microbial-induced carbonate precipitation. Transp Porous Media 87:397–420

43. Xiao Y, Liu H, Chen Q, Ma Q, Xiang Y, Zheng Y (2017) Particle breakage and deformation of carbonate sands with wide range of densities during compression loading process. Acta Geotech 12:1177–1184

44. Xiao P, Liu H, Xiao Y, Stuedlein AW, Evans TM (2018) Liquefaction resistance of bio-cemented calcareous sand. Soil Dyn Earthq Eng 107:9–19

45. Xiao Y, Stuedlein AW, Chen Q, Liu H, Liu P (2018) Stress-strain-strength response and ductility of gravels improved by polyurethane foam adhesive. J Geotech Geoenviron Eng 144:04017108

46. Xiao Y, Yuan Z, Chu J et al (2019) Particle breakage and energy dissipation of carbonate sands under quasi-static and dynamic compression. Acta Geotech 14:1741–1755

47. Xiao Y, Chen H, Stuedlein AW et al (2020) Restraint of particle breakage by biotreatment method. J Geotech Geoenviron Eng 146:04020123

48. Zhang X, Chen Y, Liu H, Zhang Z, Ding X (2020) Performance evaluation of a MICP-treated calcareous sandy foundation using shake table tests. Soil Dyn Earthq Eng 129:105959

49. Zhao B, Wang J, Coop MR, Viggiani G, Jiang M (2015) An investigation of single sand particle fracture using X-ray micro-tomography. Géotechnique 65:625–641

50. Zhou B, Ku Q, Wang H, Wang J (2020) Particle classification and intra-particle pore structure of carbonate sands. Eng Geol 279:105889

Publisher's Note Springer Nature remains neutral with regard to jurisdictional claims in published maps and institutional affiliations.